



## Sulfonates-PMMA nanoparticles conjugates: A versatile system for multimodal application

Claudio Monasterolo<sup>a</sup>, Marco Ballestri<sup>a</sup>, Giovanna Sotgiu<sup>a</sup>, Andrea Guerrini<sup>a</sup>, Paolo Dambruoso<sup>a</sup>, Katia Sparnacci<sup>d</sup>, Michele Laus<sup>d</sup>, Michelandrea De Cesare<sup>b</sup>, Assunta Pistone<sup>a</sup>, Giovanni Luca Beretta<sup>b</sup>, Franco Zunino<sup>b</sup>, Valentina Benfenati<sup>c</sup>, Greta Varchi<sup>a,\*</sup>

<sup>a</sup> Istituto per la Sintesi Organica e la Fotoreattività, 'CNR-I.S.O.F.', Area della Ricerca di Bologna, via P. Gobetti 101, 40129 Bologna, Italy

<sup>b</sup> Dipartimento di Oncologia Sperimentale e Medicina Molecolare, Fondazione IRCCS Istituto Nazionale Tumori, 20133 Milano, Italy

<sup>c</sup> Istituto per lo studio dei Materiali Nanostrutturati, ISMN Area della Ricerca di Bologna, via P. Gobetti 101, 40129 Bologna, Italy

<sup>d</sup> Dipartimento di Scienze dell'Ambiente e della Vita, Università del Piemonte Orientale 'A. Avogadro', Viale T. Michel 11, 15100 Alessandria, Italy

### ARTICLE INFO

#### Article history:

Received 13 June 2012

Revised 7 September 2012

Accepted 13 September 2012

Available online 21 September 2012

#### Keywords:

PMMA

Nanoparticles

Drug delivery

Organic dyes

Theranostic systems

### ABSTRACT

We report herein the viability of a novel nanoparticles (NPs) conjugated system, namely the attachment, based on ionic and hydrophobic interactions, of different sulfonated organic salts to positively charged poly(methylmethacrylate) (PMMA)-based core-shell nanoparticles (EAO) having an high density of ammonium groups on their shells. In this context three different applications of the sulfonates@EAO systems have been described. In detail, their ability as cytotoxic drugs and pro-drugs carriers was evaluated in vitro on NCI-H460 cell line and in vivo against human ovarian carcinoma IGROV-1 cells. Besides, 8-hydroxypyrene-1,3,6-trisulfonic acid, trisodium salt (HPTS) was chosen for NPs loading, and its internalization as bioimaging probe was evaluated on Hep G2 cells. Overall, the available data support the interest for these PMMA NPs@sulfonates systems as a promising formulation for theranostic applications. In vivo biological data strongly support the potential value of these core-shell NPs as delivery system for negatively charged drugs or biologically active molecules. Additionally, we have demonstrated the ability of these PMMA core-shell nanoparticles to act as efficient carriers of fluorophores. In principle, thanks to the high PMMA NPs external charge density, sequential and very easy post-loading of different sulfonates is achievable, thus allowing the preparation of nanocarriers either with bi-modal drug delivery behaviour or as theranostic systems.

© 2012 Elsevier Ltd. All rights reserved.

### 1. Introduction

Nanotechnology<sup>1</sup> is an enabling technology that deals with nano-meter sized objects. One of the most attractive and promising applications of nanotechnology is the use of nanomaterials in biology. Fluorescent biological labels<sup>2</sup> and drug and gene delivery<sup>3</sup> are only few examples of the possible nanomaterials applications in the field.

Improving the therapeutic index of drugs is one of the major research areas especially for anticancer, anti-inflammatory and anti-infective drugs. The majority of clinically used drugs are low-molecular weight compounds (typically under 500 gmol<sup>-1</sup>), that exhibit a short half-life in the blood stream, a high overall clearance rate and most of them show poor pharmacokinetic properties. Furthermore, they diffuse rapidly into healthy tissues and are distributed evenly within the body. As a consequence, relatively small amounts of the drug reach the target site, and therapy

is associated with serious side effects. A number of macromolecular delivery systems are under investigation to circumvent these limitations. Attaching drugs to polymeric systems has been proved to considerably modify cellular uptake with respect to the free drug. In particular this effect, which mainly consists in prolonged drug plasma half-life and more favourable pharmacokinetic, is due to the Enhanced Permeability and Retention (EPR) effect, especially for non-targeted polymer carriers.<sup>4</sup> Moreover, surface nanoparticles charge play an important role on nanospheres' interactions with cell surfaces and it has been demonstrated that, cationic particles generally exert stronger effect on cellular uptake.<sup>5</sup> On the other hand, fluorescence imaging is one of dominant detection and sensing technologies in biomedicine. At this aim, organic fluorophores are already widely used as fluorescent markers. However, they have some inherent drawbacks, such as poor resistance to photobleaching, low quantum yields and optical properties sensitive to the surrounding environments.<sup>6</sup> At this aim, researchers have encapsulated organic dyes into nano-solid matrices, such as silica,<sup>7</sup> polystyrene (PS)<sup>8</sup> and poly(methyl methacrylate) (PMMA).<sup>9</sup> With the protection of the nano-solid matrix,

\* Corresponding author. Tel.: +39 0516398283; fax: +39 0516398349.

E-mail addresses: [greta.varchi@isof.cnr.it](mailto:greta.varchi@isof.cnr.it), [g.varchi@isof.cnr.it](mailto:g.varchi@isof.cnr.it) (G. Varchi).

organic dyes can be protected from the surrounding environment, providing high photo-stability. Another advantage is that they have a higher brightness due to high number of dye molecules being loaded on one nanoparticle (NP).<sup>10</sup> Dyes and/or drugs can be loaded onto the nanoparticles according to different approaches, or combinations of them: (i) incorporated into the polymeric core, either by covalent bonds or by hydrophobic interactions; (ii) covalently bonded on the surface or, finally, (iii) electrostatically loaded on the external shell. Among these loading methodologies, covalent bonding requires a higher energy to complete the heterogeneous chemical reaction between the bioactive molecules and the matrices; moreover functional groups (such as succinimide ester or isothiocyanate or other linkers) are needed in order to achieve covalent bond formation. In contrast, NPs electrostatic post-loading needs less energy for the combination between bioactive molecules and nano-matrices, which typically occurs, in a high reproducible manner, by simple mixing the species and generally leads to higher loading ratio.<sup>11</sup> Taking into account these considerations, we explored the viability of a novel conjugated system, namely the attachment, based on ionic and hydrophobic interactions, of different sulfonated organic salts to positively charged biocompatible poly(methylmethacrylate) (PMMA)-based core-shell nanoparticles (EA0) having a high density of ammonium groups on their shells. Similar nano-systems have been previously employed for the low dose delivery of 2'-O-methyl-phosphorothioate AON, demonstrating dystrophin expression restoration in body-wide striated muscles,<sup>12</sup> and for the effective delivery of a cisplatin derivative, namely  $[\text{PtCl}_3(\text{NH}_3)]^-$ , showing very promising biological activity in C57B/6 mice bearing B16 murine melanoma.<sup>13</sup> With the aim to extend the scope of these NPs systems for drug delivery and/or for fluorescence imaging purpose, we report herein the electrostatic loading of several kinds of sulfonates salts onto EA0 along with the leakage extent of these molecules from the charged PMMA matrices. In this context three different applications of the sulfonates@EA0 systems will be described. In detail, their ability as cytotoxic drugs and pro-drugs carriers was evaluated *in vitro* on human non-small cell lung cancer carcinoma cell line NCI-H460 and *in vivo* against human ovarian carcinoma IGROV-1 cells. Besides, 8-hydroxypyrene-1,3,6-trisulfonic acid, trisodium salt (HPTS) was chosen for NPs loading and its internalization as bioimaging probe was evaluated on Hep G2 liver hepatocellular carcinoma cells, by means of confocal microscopy. HPTS was chosen because it is a highly water-soluble dye compound<sup>14</sup> with low toxicity,<sup>15</sup> and it is also very cheap compared with most other indicators. Furthermore, this tri- or tetra-anionic dye is retained well inside living cells at physiological pH values and it has been used for measurement of cytoplasmic pH in many cell types,<sup>16</sup> or acidic organelle pH.<sup>17</sup> The main limitation to the use of HPTS as an intracellular indicator is its lack of cell permeability, and there is no convenient pro-drug-like form to facilitate transport of this dye into cells.<sup>18</sup>

## 2. Experimental details

### 2.1. Materials

2-(Dimethylamino)ethyl methacrylate (DMAEMA), 1-bromoocane, 2,2'-azobis(2-methylpropionamide) dihydrochloride (AIBA), methyl methacrylate (MMA, 99.0%) (distilled before use) and HPTS were purchased from Sigma-Aldrich. Hep G2 cell line were generously provided by Istituto Scientifico Romagnolo per lo Studio e la cura dei Tumori (IRST) of Meldola (FC, Italy).

### 2.2. Analytical measurements and methods

The hydrodynamic diameter of the nanospheres was determined by dynamic light scattering (DLS) at 25 °C using a Zetasizer 3000 HS system (Malvern, UK) equipped with a 10 mV He-Ne laser. As far as the electrophoretic mobility is concerned,  $\zeta$ -potential was measured at 25 °C by means of the same Zetasizer system. The instrument calibration was checked using standard polystyrene latexes, supplied by Malvern Instruments with known zeta-potential. To achieve a constant ionic background, the samples were diluted with 1.0 mM KCl solutions to a concentration of 20  $\mu\text{g}/\text{ml}$ . Each value is the average of five measurements. The quaternary ammonium group load per gram of nanosphere was determined by potentiometric titration of the bromide ions obtained after complete ion exchange. The compound@EA0 samples were isolated from the solution in which were suspended (both during the synthesis, the loading and release experiments) by means of the Eppendorf vials and a EBA 12 HETTIC centrifuge equipped with a F-205 FALC tubes rotator. The release amount was determined by spectrophotometric measures with a Lambda 20 Perkin Elmer spectrophotometer. Supernatants were filtered by an Amicon Ultra 0.5 ml 100 K Millipore Filter. The positively charged nanospheres were obtained by emulsion polymerization of methyl methacrylate in the presence of the ionic co-monomer 2-(dimethyloctyl) ammonium ethylmethacrylate bromide as emulsion stabilizer. A more detailed description of the NPs synthesis is reported in the ESI material.

### 2.3. Loading and release experiments

**Loading.** Briefly, sulfonates were combined with EA0 nanoparticles by electrostatic interaction: a certain amount of sulfonate derivative (typically 50–600  $\mu\text{g}/\text{mL}$  in  $\text{mQ H}_2\text{O}$ ), was added to an aqueous solution of positively charged EA0 (5  $\text{mg}/\text{mL}$ ) and stirred in a Vortex apparatus for 20 s. at room temperature. Each sample was then centrifuged (4 min, 16597 RCF) and the supernatant was filtered with a 0.1  $\mu\text{m}$  filter (1 min 10622 RCF). The filtrate was analyzed with a Lambda 20 Perkin Elmer Spectrophotometer at the correct wavelength, thus for each compound a calibration curve was generated for further determination of the loading values.

**Release.** Sulfonates release from EA0 was measured by spectrophotometric analysis according to two different procedures: as a function of the washing solution, or as a function of time by using the same washing solution. Typically, a precise sulfonate-EA0 sample amount was treated with the washing solution, which was added to restore the initial volume (typically 500 mL). In particular, phosphate buffer saline (PBS) and PBS plus different amounts of NaCl were employed as release solutions. Experiments were performed either at room temperature or at 37 °C. The sample was then re-suspended by vortexing it (20 s) and then centrifuged (4 min, 16597RCF). The supernatant was filtered with a 0.1  $\mu\text{m}$  filter (1 min 10622 RCF). The filtrate was analysed by spectrophotometric measure.

### 2.4. In vitro biological assay

The human non-small cell lung cancer carcinoma cell line NCI-H460 (ATCC, HTB-177) was cultured in RPMI-1640 containing 10% foetal calf serum. Cytotoxicity was assessed by growth inhibition assay after 72 h drug exposure. Cells in the logarithmic phase of growth were harvested and seeded in duplicates into 6-well plates. Twenty four hours after seeding, cells were exposed to the drug for

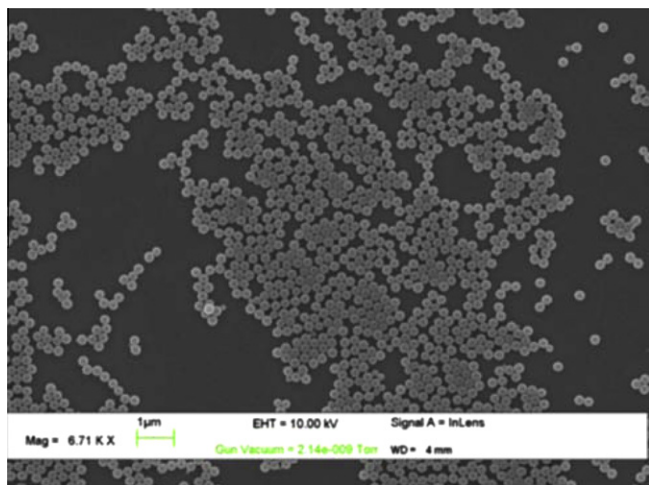


Figure 1. SEM micrograph of EA0.

72 h and counted with a Coulter counter.  $IC_{50}$  is defined as the inhibitory drug concentration causing a 50% decrease of cell growth over that of untreated control.

### 2.5. In vivo biological assay

Female athymic Swiss nude mice, 7–10 weeks old (Charles River, Calco, Italy) were used. Mice were maintained in laminar flow rooms, keeping temperature and humidity constant. Mice had free access to food and water. Experiments were approved by the Ethics Committee for Animal Experimentation of the Fondazione IRCCS Istituto Nazionale Tumori of Milan according to institutional guidelines.<sup>19</sup> Exponentially growing human IGROV-1 ovarian carcinoma cells<sup>20</sup> ( $10^7$  per mouse) were sc injected into the right flank of athymic nude mice. Tumor lines were achieved by serial sc passages of fragments from growing tumors into healthy mice as described previously.<sup>21</sup> Tumor growth was followed by biweekly measurements of tumor diameters with a Vernier caliper. Tumor volume (TV) was calculated according to the formula:  $TV (\text{mm}^3) = d^2 \times D/2$ , where  $d$  and  $D$  are the shortest and longest diameters, respectively. Drugs were delivered iv every day for four times starting when tumors were in the range of 50 to  $100 \text{ mm}^3$ . Experimental groups were eliminated when mean TV was about  $1500 \text{ mm}^3$ . The efficacy of drug treatment was assessed as: tumor weight inhibition percentage (TWI%) in treated versus control mice, calculated as:  $TWI\% = 100 - (\text{mean TW treated}/\text{mean TW control} \times 100)$ . The toxicity of the drug treatment was determined as lethal toxicity. Deaths occurring in treated mice before the death of the first control mouse were ascribed to toxic effects.

### 2.6. HepG2 cell culturing, treatment and imaging

HepG2 cells has been cultured in T25 cell culture flasks containing Dulbecco's Modified Eagle Media (DMEM)/HAM's-F12 (1:1) supplemented with 10% v/v of Fetal Bovine Serum, 1% L-glutamine, 1% insulin and antibiotics (penicillin/streptomycin (100 U/ml and 100  $\mu\text{g}/\text{ml}$ , respectively). Culture flasks were maintained in a humidified incubator with 5%  $\text{CO}_2$  at 37 °C and cells has been split every third day. The day before experiment cells has been re-plated on 19 mm coverslips coated with poly-D-lysine, placed into 12-multiwell plate at a concentration of  $5 \times 10^3$  per sample. PMMA-NPs, HPTS and HPTS@PMMA-NPs have been added to cell culture media from respective sterile aqueous stock solutions at a minimum dilution factor of 1:100. After 24 h of incubation, all the sam-

ples have been washed for three times with PBS media before performing imaging experiments. Optical imaging has been performed with a Nikon TE 2000 inverted microscope equipped with a 20 $\times$  and 60 $\times$  objective and Hamamatsu CCD camera. Fluorescence images were collected at 515 nm, exciting samples with mercury lamp at 450 nm. Coverslips were then mounted by means of a customs made chamber onto Nikon TE 2000 inverted confocal microscope equipped with a 20 $\times$  or 60 $\times$  oil-objective and 400 nm diode, 488 nm Ar<sup>+</sup> and 543 nm He-Ne lasers as excitation sources. Images reported are representative of 2 different experiments performed in triplicate.

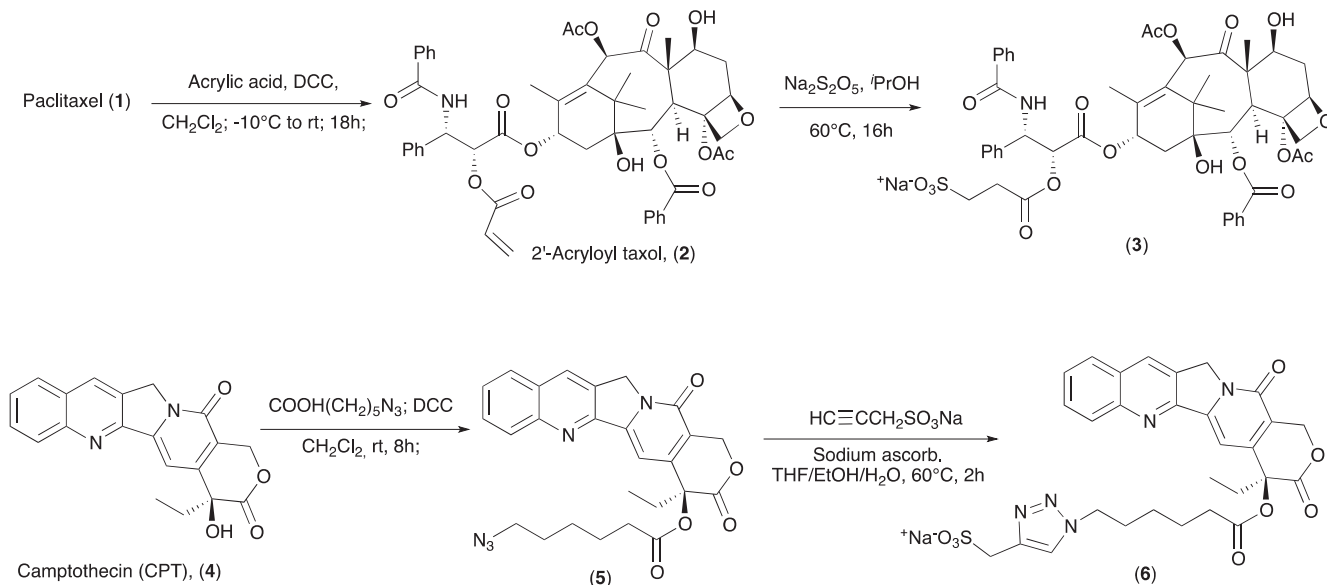
## 3. Results and discussion

### 3.1. Synthesis of core-shell PMMA NPs (EA0)

As reported for many emulsion polymerization systems that include water-soluble co-monomers, the reaction starts in the aqueous phase leading to the formation of water-soluble oligoradicals that are rich in the water-soluble co-monomer until they reach the solubility limit and precipitate to form primary particles, which are able to grow by the incorporation of monomer and co-monomer. The water-soluble units are preferentially located at the nanosphere surface and actively participate in latex stabilization. Nanospheres can thus be obtained with tailored surfaces dictated by the chemical structure of the co-monomer/s employed, ultimately leading to the formation of core-shell nanospheres. In particular, these biocompatible, surfactant-free polymeric core-shell nanoparticles are able to bind biologically active molecules and macromolecules on their surface.<sup>11,22</sup> EA0 nanoparticles are characterized by an average SEM diameter of  $150 \pm 40 \text{ nm}$  (Fig. 1) and by a hydrodynamic diameter, evaluated by dynamic light scattering (DLS), of 183 nm. The density of the cationic groups available for interaction with the organic sulfonates turned out to be  $0.16 \mu\text{mol}$  of quaternary ammonium groups per nanosphere's gram. Finally, the analysis of  $\zeta$ -potential (46,7 mV), which was measured after dialysis purification, confirmed that the cationic co-monomer employed in the polymerization reaction is covalently bound to the nanoparticle surface. The difference in the NPs radii observed with PCS and SEM techniques could be ascribed to the different environments in which the measurements are performed, for example, water and air, respectively. The Stokes diameter measured with PCS corresponds to the size of the solvated nanoparticle, which is enhanced due to the presence of the external ammonium groups; while SEM directly measure the dry radius.

### 3.2. Synthesis of taxol and camptothecin sulfonates

With the purpose of evaluating drugs-polymers conjugates, we selected two conveniently tailored camptothecin (CPT) and taxol analogues, respectively. CPT (**4**) is a natural product that exerts cytotoxic activity through the inhibition of topoisomerase I leading to cell death; unfortunately, under physiological conditions, the high in vivo reactive  $\alpha$ -hydroxy- $\delta$ -lactone pharmacophore, reversibly hydrolyses to the inactive and toxic 'ring opened' carboxylate form, making it inadequate for therapy.<sup>23</sup> Paclitaxel (**1**) and its analogs are currently recognized as the most important available drugs for treatment of solid tumors,<sup>24</sup> albeit these compounds present relevant drawbacks, such as poor solubility, lack of tumor cells selectivity<sup>25</sup> and drug resistance expression. Following Kingston's procedure<sup>26</sup> we first synthesized a taxol sulfonate analogue (**3**, Scheme 1). Kingston and coworkers demonstrated that this water-soluble analogue of taxol has in vitro and in vivo activity, close to the parent compound, towards P-388 lymphocytic



**Scheme 1.** Taxol and CPT sulfonate derivatives synthesis.

leukemia. CPT-sulfonate derivative **6** (Scheme 1) was straightforwardly synthesized from CPT (see supplementary information for synthesis details).

### 3.3. Loading and release experiments

As reported in Table 1, along with taxol and camptothecin sulfonate derivatives (**3** and **6**, respectively), we also employed some thiophene based organic dyes (**7–9**), and commercially available 8-hydroxypyrene-1,3,6-trisulfonic acid, trisodium salt (HPTS, **10**) (Table 1). Binding experiments exhibited different loading capacity, mainly depending on sulfonate properties, such as medium solubility, molecular weight and steric hindrance. The release of sulfonates from EA0 was evaluated in water, phosphate buffer solution (PBS), which roughly mimics physiological conditions,<sup>27</sup> and PBS containing different sodium chloride (NaCl) concentrations. Release experiments provided different results depending on the sulfonate: thiophenes based organic dyes (**7–9**) showed very poor release efficiency, while HPTS was not released from the NPs even after repeated washing, maybe due to the presence of three sulfonate groups and/or to the system steric hindrance. It is worth noting that very recently, Xu and coworkers reported a similar approach for the synthesis of fluorescent dyes loaded PMMA nanospheres by electrostatic adsorption.<sup>28</sup> In that case fluorescein sodium salt, Rhodamine 6G and Rhodamine B were employed as dyes. Compared to those examples, the use of a reactive surfactant for EA0 synthesis, allows the formation of a highly positively charged shell, which in turn provide a much higher loading capability with no release of the dye from the nanospheres, as also confirmed from confocal images (Fig. 4). Moreover, compared to other micro- and nano-spheres in which cationic surfactants are able to adsorb drugs onto particles' surface,<sup>29</sup> our system does not suffer from inherent surface instability, e.g. cationic surfactant desorption, thus leading to high reproducibility and lower toxic effects incidence.

The opportunity to suitably modulate the bioactive molecule release from the nanoparticle shell, represent a very interesting characteristic in the field of theranostic nanomedicine, which relates to the development of an integrated nano-therapeutic system, which can diagnose, deliver targeted therapy and monitor the response. With particular reference to taxol and CPT derivatives,

compound **3** showed a maximum loading value of 61.6 mg/mg, while for compound **6** the highest loading value was of 72.6 mg/mg, thus revealing a loading efficiency of 38% and 72%, respectively. This parameter was determined by comparing the highest mmol quantity of compound loaded on the nanospheres with the effective density of cationic groups present on the nanoparticles (0.16 mmol/mg).

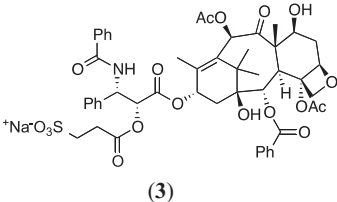
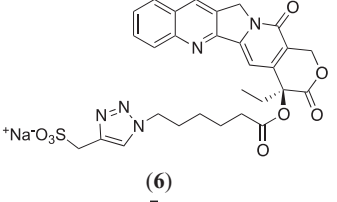
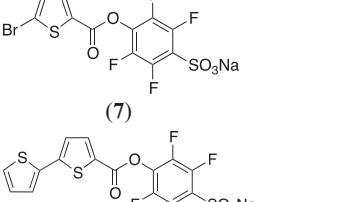
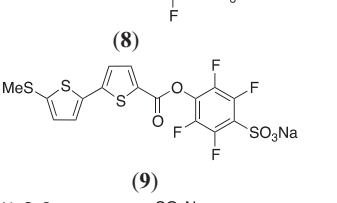
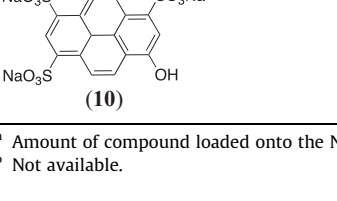
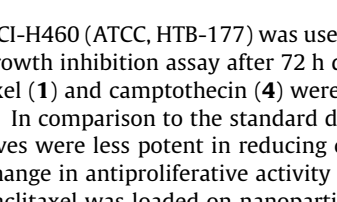
The stability of **3**@EA0 and **6**@EA0 adducts was evaluated by subsequent treatment with different washing solutions, such as water, PBS and PBS containing different concentrations of NaCl. In particular, Figure 2A shows that, starting from a sample of **3**(or **6**)@EA0 at a concentration of 40  $\mu\text{g}_{\text{compound}}/\text{mg}_{\text{particle}}$  and performing successive washes of the same samples, a gradual release of the compound occurs. While little release is observed when using pure water, it becomes much more pronounced when using PBS. The chart also clearly indicates the greater tendency of the CPT derivative to be released in phosphate buffer conditions.

In order to assess the release degree of the compound over time, samples of **3**@EA0 and **6**@EA0 (40  $\mu\text{g}_{\text{compound}}/\text{mg}_{\text{particle}}$ ) were treated with PBS at 37 °C for 30 h. Residual loading of the compounds has been determined by spectrophotometric analysis of aliquots of the solutions collected at regular intervals (Fig. 2B). Time-dependent experiments confirmed the higher tendency of the CPT derivative to be released from the NPs with respect to the taxol one, that is, 70% and 30% respectively after 2.5 h. NaCl addition to the washing solution does not alter the release trend for **3**@EA0, unless it reaches a concentration of at least 2 M, when we observed a radical release drop, maybe because a high  $\text{Cl}^-$  concentration prevent phosphates to replace the drug on the polymer (Fig. 2C). Overall, experimental data showed a continuous release of the drugs, which afterwards reaches a plateau, and a small amount of drug seems to remain tightly associated to the nanospheres. These analytical results prompted us to further explore the behavior of these nano-sized systems *in vitro* and *in vivo* tumor environment.

### 3.4. In vitro biological assay

*In vitro* studies were conducted on both **3**@EA0 and **6**@EA0 core-shell nanoparticles conjugates to evaluate their therapeutic performance. The human non-small cell lung cancer carcinoma cell line

**Table 1**  
Sulfonates loading experiments on EA0 nanoparticles

Loaded compounds	Loading solutions ( $\mu\text{g/mL}$ )				
	50	100	200	300	600
 <p>(3)</p>	9.76 <sup>a</sup>	19.6	38.9	51.8	61.6
 <p>(6)</p>	9.72	19.4	38.5	59.9	72.6
 <p>(7)</p>	10.2	19.9	33.7	33.3	31.1
 <p>(8)</p>	10	20	39.2	56.8	60
 <p>(9)</p>	9.99	20	38.7	45.3	52.2
 <p>(10)</p>	10	20	40	na <sup>b</sup>	na <sup>b</sup>

<sup>a</sup> Amount of compound loaded onto the Nps ( $\mu\text{g/mg}$ ) obtained by varying the concentration of the loading solutions.

<sup>b</sup> Not available.

NCI-H460 (ATCC, HTB-177) was used. Cytotoxicity was assessed by growth inhibition assay after 72 h drug exposure. (Table 2) Paclitaxel (**1**) and camptothecin (**4**) were used as references.

In comparison to the standard drugs, the two sulfonate derivatives were less potent in reducing cell growth (**1** vs **3**, **4** vs **6**). No change in antiproliferative activity was evidenced when sulfonate paclitaxel was loaded on nanoparticles (**3** vs **3@EA0**). On the contrary, loading of **6** on the pellets was detrimental for its potency (**6** vs **6@EA0**). The very poor in vitro cytotoxicity of **6** suggests that this derivative might act as a prodrug, thus requiring an enzyme action to release the bioactive CPT, but more studies are needed to establish if **6@EA0** conjugated can behave as a carrier-prodrug system.

### 3.5. In vivo biological assay

In an attempt to explore possible therapeutic advantages of **3@EA0** adduct, we have performed comparative in vivo studies using paclitaxel **1** as reference. The antitumor potency was evaluated in nude mice bearing the human ovarian carcinoma IGROV-1 xenograft in 3 independent experiments. As a consequence of the relatively low amount of drug linked to the nanoparticles, a limited

dose of the drug equivalent could be administrated as iv bolus injection. With this treatment modality only 20 mg/kg (around 0.4 ml/injection) could be used, thus allowing the delivery of 15 mg/kg (Table 3). In vivo data show that the administration of **3@EA0** produced significant antitumor activity, while no effect was found for the free taxane derivative (i.e., compound **3**).

The lower efficacy of **3@EA0** in comparison to the paclitaxel may reflect an intrinsic low efficacy of the taxane analog (**3**) used for the conjugation. The in vivo lack of activity of **3** may be related to an unfavorable pharmacokinetic behavior, which seems to be overtaken when conjugation with EA0 nanospheres occurs.

### 3.6. Absorbance and fluorescence emission spectra of HPTS@EA0

Spectrophotometric analysis of the HPTS-doped PMMA NPs in water solution (Fig. 3) revealed the same emission and absorption maxima of the free fluorophore, thus indicating that the loaded dye preserves its spectroscopic characteristics. These results, along with cell imaging experiments (see point 3.7), suggest that the HPTS@EA0 could be exploited as novel and effective pH responsive nano-sensor, given that HPTS is well known for measurement of

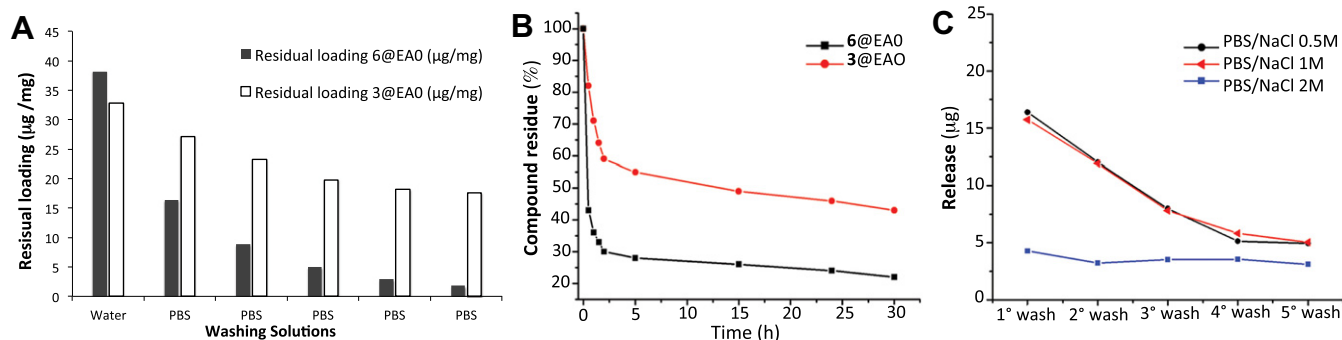


**Figure 2.** Release experiments. (A) Conditions: initial concentration [ $6@EA0$ ] = [ $3@EA0$ ] =  $40 \mu\text{g}_{\text{compound}}/\text{mg}_{\text{particle}}$ ; washing solution: water followed by PBS; the chart reports the residual amount of compound loaded on the NPs ( $40 \mu\text{g}/\text{mg}_{\text{particle}}$ ) after the wash (■ for  $6@EA0$  and □ for  $3@EA0$ ). (B) Conditions: initial concentrations: [ $6@EA0$ ] = [ $3@EA0$ ] =  $40 \mu\text{g}_{\text{compound}}/\text{mg}_{\text{particle}}$ ; washing solution: PBS a  $37^\circ\text{C}$ . (C) Conditions: initial concentrations: [ $3@EA0$ ] =  $40 \mu\text{g}_{\text{compound}}/\text{mg}_{\text{particle}}$ ; washing solutions: PBS/NaCl 0.5 M,  $37^\circ\text{C}$ ; PBS/NaCl 1 M,  $37^\circ\text{C}$ ; PBS/NaCl 2 M,  $37^\circ\text{C}$ .

**Table 2**  
Antiproliferative activity of  $3@EA0$  and  $6@EA0$ <sup>a</sup>

Entry	Compound	IC <sub>50</sub> (µM)
1	Paclitaxel ( <b>1</b> )	$0.046 \pm 0.012$
2	<b>3</b>	$0.076 \pm 0.011$
3	$3@EA0$	$0.080 \pm 0.062$
4	CPT ( <b>4</b> )	$0.0014 \pm 0.00014$
5	<b>6</b>	$0.113 \pm 0.0099$
6	$6@EA0$	$0.333 \pm 0.142$

<sup>a</sup> IC<sub>50</sub>, drug concentration required for 50% reduction of cell growth as compared with untreated controls after 72-h exposure to the drug. Means  $\pm$  SD are reported from at least three experiments.

**Table 3**  
Antitumor activity of  $3@EA0$  on the IGROV-1 ovarian carcinoma xenografted in nude mice

Entry	Drug	Dose (mg/kg)	Days treatment	TWI <sup>a</sup> (%)	Tox <sup>b</sup>
1	<b>1</b>	15	3,4,5,6	91 (13) <sup>*</sup>	0/4
2	<b>3</b>	15	3,4,5,6	0	0/4
3	$3@EA0$	15	3,4,5,6	44 (13) <sup>*</sup>	0/4

<sup>\*</sup>  $P < 0.05$  by Student's *t* test versus control mice.

<sup>a</sup> Tumor weight inhibition percentage in treated over control mice, in parenthesis the day on which it was assessed.

<sup>b</sup> Dead/treated mice.

cytoplasmic pH in many cell types,<sup>16</sup> or acidic organelle pH.<sup>17</sup> The use of this NPs system could allow to overcome the main limitation associated with the use of free HPTS as intracellular pH indicator, that is, the high lack of cell permeability.

### 3.7. HepG2 cell culturing, treatment and imaging

To verify capability of PMMA-NPs to promote cellular internalization of water soluble dye such as HPTS, HepG2 cells have been incubated with PMMA-NPs, HPTS, and HPTS@NPs for 24 h. After washing the sample three times with PBS media, we performed fluorescence optical microscopy and confocal microscopy. Optical images and fluorescence images, collected at 515 nm, exciting samples with mercury lamp at 450 nm, revealed that most of the HepG2 cells treated with 500 ng/mg HPTS@NPs (Fig. 4A and B) were fluorescently labelled, whereas no fluorescent signal was emitted by cells treated with the same concentration of unloaded HPTS (Fig. 4C and D) nor by cells treated with PMMA-NPs (See Supplementary Fig. S3A and B). Confocal imaging of the same samples indicates that HepG2 cells treated with 500 ng/mg HPTS@NPs (Fig. 4E and F) and 200 ng/mg HPTS@NPs (See Supplementary

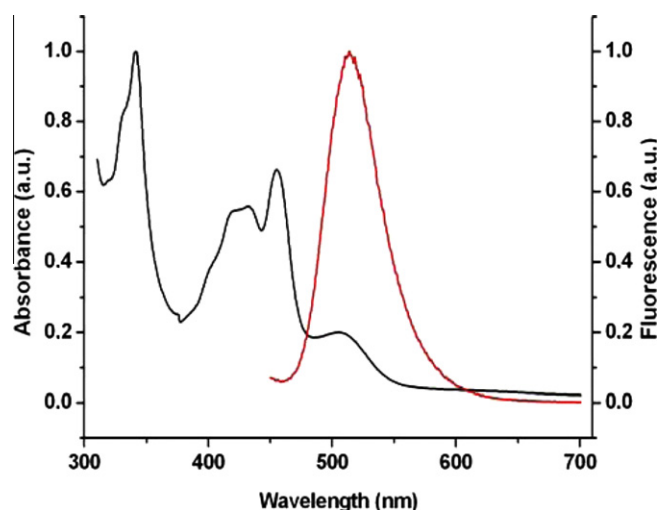


**Figure 3.** Absorption and emission spectra of HPTS@EA0 in water.

Fig. S3C and D) displayed mostly diffuse fluorescence, even though granular fluorescence was also visible at higher magnification (Fig. 4F, arrows).

Collectively these data demonstrated that the loading of HPTS on PMMA-NPs enable water-soluble dye internalization in HepG2 cells and suggested that intracellular localization of the nanoparticles could occur in the cytoplasm as well as in endocytic vesicles.

The main advantage of our system, compared to previously reported ones,<sup>27</sup> mainly consists in the easiness of its preparation, e.g. by simply mixing the proper amounts of NPs and fluorophore. More studies will be carried out to demonstrate this feature.

### 4. Conclusions

In summary, the available data support the interest for these PMMA nanoparticles-sulfonates conjugated systems as a promising formulation for theranostic applications. In fact, we demonstrated that sulfonates release can be efficiently modulated based on molecules steric hindrance and on the number of sulfonate groups. This behavior allows exploiting PMMA-NPs@sulfonate systems either for slow release of drugs and pro-drugs, or for efficient cell internalization of imaging dyes or for their combined use. The easy functionalization of bioactive molecules with sulfonates groups by means of straightforward and high yielding synthetic methodologies,<sup>30</sup> paves the way to a wide range of applications in terms of drug (pro-drugs) delivery and diagnosis tools.

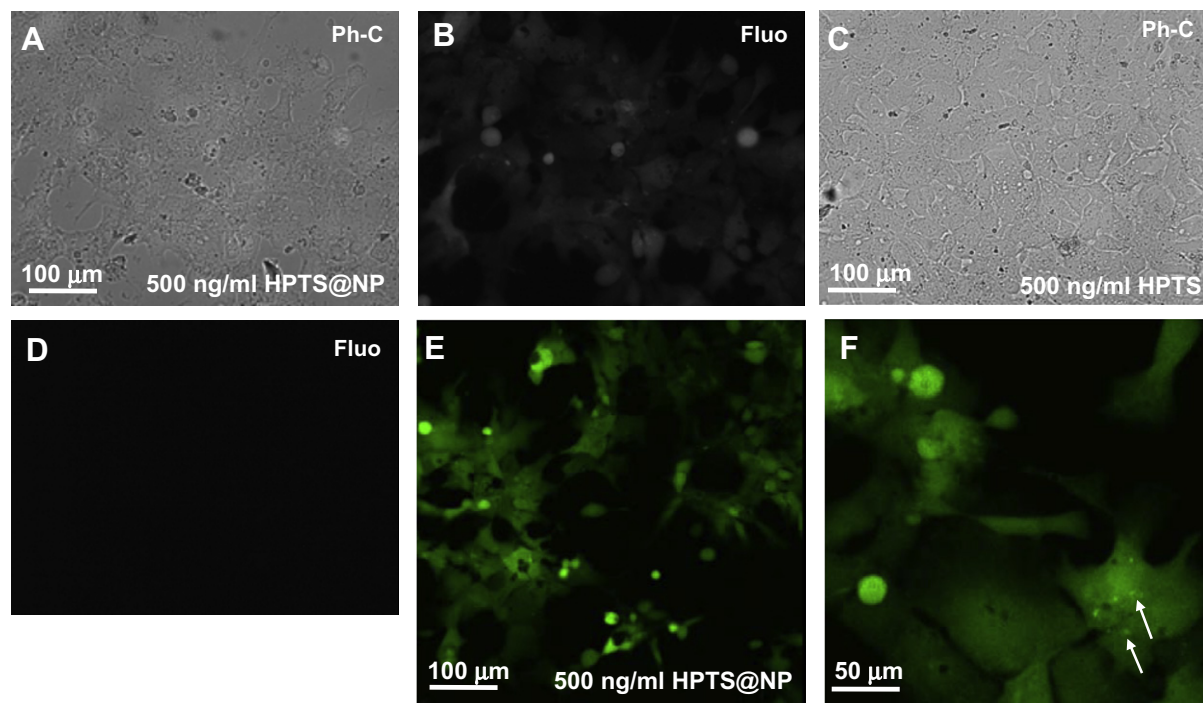


**Figure 4.** (A–D) Phase Contrast (Ph-C, A,C) and relative fluorescent (fluo, B,D) micrographs collected from HepG2 cells treated with 500 ng/ml HPTS@NPs. (E) Low magnification ( $20\times$ ) (A and B) and 500 ng/ml HPTS (C and D). Scale bar is 100  $\mu\text{m}$ . (E) single plane confocal image representative of fluorescent emission collected by HepG2 cells after 24 h of incubation with 500 ng/ml HPTS@NPs. (F) higher magnification of the same sample revealed that cells exhibit mostly diffuse but also granular fluorescence pattern (white arrows).

Moreover, the great versatility of the nanoparticles synthesis, allows to easily obtain nano-matrix with different degree of external charges and with sizes ranging from 20 nm to 1  $\mu\text{m}$ . Furthermore, a fine tuning of the polymerization parameters, such as the nature of the monomer, of the co-monomer and their relative amounts, allows the further external shell functionalization, which could be extremely useful for the covalent attachment of target moieties, for example, peptides, antibodies, etc. Overall, in vivo biological data strongly support the potential value of these core-shell nanoparticle as delivery system for negatively charged drugs or biologically active molecules. The administration of the nanoparticles by slow infusion is expected to improve the efficacy. Relevant to this point is the good tolerability of this novel drug formulation. These results confirm the potential of the PMMA core-shell nanoparticles as drug carriers, previously reported by Osella and coworkers,<sup>11</sup> by extending the scope of these systems to a more wide range of molecules. Additionally, we have demonstrated the ability of these PMMA core-shell nanoparticles to act as efficient carriers of fluorophores. In particular, the electrostatic irreversible attachment of HPTS on the outer NPs shell, allows the efficient internalization of the dye, thus introducing new chances for cellular uptake of negatively charged fluorophores and their possible use as nanosensors. In principle, thanks to the high PMMA NPs external charge density, sequential post-loading of different sulfonates is achievable, thus allowing the preparation of nanocarriers either with bi-modal drug delivery behaviour, e.g., loading two different drugs with diverse action modes, or as theranostic systems, for example, for diagnosis, drug-delivery and response monitoring. Investigation of these possibilities is actively underway in our laboratories.

#### Acknowledgments

Mediteknology S.r.l., Area Ricerca CNR, Via Gobetti 101, I-40129 Bologna, Italy for kindly providing compounds **6–8**. This work was

also supported by Italian MIUR project FIRB-RBPR05JH2 (ITALNANONET).

#### Supplementary data

Supplementary data associated with this article can be found, in the online version, at <http://dx.doi.org/10.1016/j.bmc.2012.09.023>.

#### References and notes

- Feynman, R. *Science* **1991**, *254*, 1300.
- (a) Chan, W. C. W.; Nie, S. M. *Science* **1998**, *281*, 2016; (b) Wang, S.; Mamedova, N.; Kotov, A.; Chen, W.; Studer, J. *Nano Lett.* **2002**, *2*, 817.
- Panatarotto, D.; Pridos, C. D.; Hoebeke, J.; Brown, F.; Kramer, E.; Briand, J. P.; Muller, S.; Prato, M.; Bianco, A. *Chem. Biol.* **2003**, *10*, 961.
- (a) Matsumura, Y.; Maeda, H. *Cancer Res.* **1986**, *46*, 6387; (b) Iyer, A.; Khaled, G.; Fang, J.; Maeda, H. *Drug Discovery Today* **2006**, *11*, 812.
- (a) Nel, A. E.; Mädler, L.; Velegol, D.; Xia, T. E.; Hoek, M.; Somasundaran, P.; Klaessig, F.; Castranove, V.; Thompson, M. *Nat. Mater.* **2009**, *8*, 543; (b) Fleck, C. C.; Netz, R. R. *Europhys. Lett.* **2004**, *67*, 314.
- (a) Zhou, X.; Zhou, J. *Anal. Chem.* **2004**, *76*, 5302; (b) Ma, D. L.; Kell, A. J.; Tan, S.; Jakubek, Z. J.; Simard, B. J. *Phys. Chem. C* **2009**, *113*, 15974.
- (a) Andrew, A. B.; Jelena, V.; Hooisweng, O.; Erik, H.; Oula, P. M.; Martin, B.; Steven, M. L.; Ulrich, W.; Michelle, B. *Nano Lett.* **2009**, *9*, 442; (b) Liang, S.; John, C. L.; Xu, S. P.; Chen, J.; Jin, Y. H.; Yuan, Q.; Tan, W. H.; Zhao, J. X. J. In *Silica-Based Nanoparticles: Design and Properties Advanced Fluorescence Reporters in Chemistry and Biology II*; Demchenko, A., Ed.; Springer: Berlin, 2010; p 229.
- Wittmershaus, B. P.; Skibicki, J. J.; McLafferty, J. B.; Zhang, Y. Z.; Swan, S. J. *Fluoresc.* **2001**, *11*, 119.
- (a) Melanie, B.; Muthupandian, A.; Franz, G. J. *Am. Chem. Soc.* **2003**, *125*, 525; (b) Bosma, G.; Pathmamanoharan, C.; Hoog, E. H. A. D.; Kegel, W. K.; Blaaderen, A. V.; Lekkerkerker, H. N. W. J. *Colloid Interface Sci.* **2002**, *245*, 292.
- (a) Yao, G.; Wang, L.; Wu, Y. R.; Smith, J.; Xu, J. S.; Zhao, W. J.; Lee, E. J.; Tan, W. H. *Anal. Bioanal. Chem.* **2006**, *385*, 518; (b) Rampazzo, E.; Bonacchi, S.; Montalti, M.; Prodi, L.; Zaccheroni, N. J. *Am. Chem. Soc.* **2007**, *129*, 14251.
- Wang, S.; Fan, W.; Kim, G.; Jin Hah, H.; Koo Lee, Y.-E.; Kopelman, R.; Ethirajan, M.; Gupta, A.; Goswami, L. N.; Pera, P.; Morgan, J.; Pandey, R. K. *Lasers Surg. Med.* **2011**, *43*, 686.
- Rimessi, P.; Sabatelli, P.; Fabris, M.; Braghetta, P.; Bassi, E.; Spitali, P.; Vattemi, G.; Tomelleri, G.; Mari, L.; Perrone, D.; Medici, A.; Neri, M.; Bovolenta, M.; Martoni, E.; Maraldi, N. M.; Gualandi, F.; Merlini, L.; Ballestri, M.; Tondelli, L.; Sparnacci, K.; Bonaldo, P.; Caputo, A.; Laus, M.; Ferlini, A. *Mol. Ther.* **2009**, *17*, 820.

13. Monti, E.; Gariboldi, M. B.; Ravizza, R.; Molteni, R.; Sparnacci, K.; Laus, M.; Gabano, E.; Ravera, M.; Osella, D. *Inorg. Chim. Acta* **2009**, 362, 4099.
14. Zhang, Z.; Seitz, W. R. *Anal. Chim. Acta* **1984**, 160, 47.
15. Wolfbeis, O. S.; Fuerlinger, E.; Kroneis, H.; Marsoner, H.; Fresenius', Z. *Anal. Chem.* **1983**, 314, 119.
16. Giuliano, K. A.; Gillies, R. J. *Anal. Biochem.* **1987**, 167, 362.
17. Overly, C. C.; Lee, K. D.; Berthiaume, E.; Hollenbeck, P. J. *Proc. Natl. Acad. Sci. U.S.A.* **1995**, 92, 3156.
18. Han, J.; Burgess, K. *Chem. Rev.* **2010**, 110, 2709.
19. Workman, P.; Balmain, A.; Hickman, J. A.; McNally, N. J.; Mitchison, N. A.; Pierrepont, C. G.; Raymond, R.; Rowlatt, C.; Stephens, T. C.; Wallace, J. *Br. J. Cancer* **1988**, 58, 109.
20. Soranzo, C.; Pratesi, G.; Zumino, F. *Anticancer Drugs* **1990**, 1, 23.
21. Polizzi, D.; Pratesi, G.; Tortoreto, M.; Supino, R.; Riva, A.; Bombardelli, E.; Zumino, F. *Cancer Res.* **1999**, 59, 1036.
22. Laus, M.; Sparnacci, K.; Lelli, M.; Vannini, R.; Tondelli, L. *J. Polym. Sci., Part A: Polym. Chem.* **2000**, 38, 1110.
23. Wall, M. E. In *Biochemie und Physiologie der Alkaloide*; Mothes, K., Schreiber, K., Eds.; Akademie Verlag: Berlin, 1969; p 77.
24. (a) Nicolau, K. C.; Dai, W. M.; Guy, R. K. *Angew. Chem., Int. Ed. Engl.* **1994**, 33, 15; (b) Menzin, A. W.; King, S. A.; Aikins, J. K.; Mikuta, J. J.; Rubin, S. C. *Cancer Gynecol. Oncol.* **1994**, 54, 103; (c) Rowinski, E. K. *Annu. Rev. Med.* **1997**, 48, 353.
25. Chari, R. V. J. *Adv. Drug Delivery Rev.* **1998**, 31, 89.
26. Zhao, Z.; Kingston, D. G. I.; Crosswell, A. R. *J. Nat. Prod.* **1991**, 54, 1607.
27. Matthews, G. G. *Cellular Physiology of Nerve and Muscle*, IV ed.; Blackwell Publishing Malden: MA, 2003. pp. 5–6.
28. Wang, X.; Xu, S.; Liang, C.; Li, H.; Sun, F.; Xu, W. *Nanotechnology* **2011**, 22, 275608.
29. (a) O'Hagan, D.; Singh, M.; Ugozzoli, M.; Wild, C.; Barnett, S.; Chen, M.; Schaefer, M.; Doe, B.; Otten, G. R.; Ulmer, J. B. *J. Virol.* **2001**, 75, 9037; (b) Oster, C. G.; Kim, N.; Grode, L.; Barbu-Tudoran, L.; Schaper, A. K.; Kaufmann, S. H. E.; Kissel, T. J. *Control Release* **2005**, 104, 359.
30. Matthews, G. G. *Cellular Physiology of Nerve and Muscle*, fourth ed.; Blackwell Publishing Malden: MA, 2003. pp. 5–6.